Scientific Research Publishing

Open Journal of Organic Polymer Materials, 2018, 8, 53-79
http://www.scirp.org/journal/ojopm
ISSN Online: 2164-5752
ISSN Print: 2164-5736

Novel Corrosion Inhibitors for Carbon Steel Alloy in Acidic Medium of 1N HCl Synthesized from Graphene Oxide

Hawraa H. Radey[1], Moayed N. Khalaf[2], Hadi Z. Al-Sawaad[2]

[1]Department of Chemistry, College of Science, University of Mysan, Basra, Iraq
[2]Department of Chemistry, College of Science, University of Basrah, Basrah, Iraq
Email: mariumkarar@yahoo.com

How to cite this paper: Radey, H.H., Khalaf, M.N. and Al-Sawaad, H.Z. (2018) Novel Corrosion Inhibitors for Carbon Steel Alloy in Acidic Medium of 1NHCl Synthesized from Graphene Oxide. *Open Journal of Organic Polymer Materials*, **8**, 53-79.
https://doi.org/10.4236/ojopm.2018.84005

Received: September 17, 2018
Accepted: October 28, 2018
Published: October 31, 2018

Copyright © 2018 by authors and Scientific Research Publishing Inc.
This work is licensed under the Creative Commons Attribution International License (CC BY 4.0).
http://creativecommons.org/licenses/by/4.0/

Open Access

Abstract

In this study, two nano-derivatives from nano-Graphene oxide (GO) were synthesized. Regarding to GON and GOS by reaction GO with 2-amino ethanol and 2-marcapto ethanol respectively, the GO, GON, GOS were characterized by FTIR, XRD and FSEM. Evaluation prepared compound to inhibitors corrosion for Carbon steel in acidic media at (1 - 6 ppm) concentration and different temperature 298, 308, 318, 328 K. The electrochemical technique used Tafel plot to measure the efficiency of inhibitor. It was observed that the corrosion rate and charge transfer of the carbon steel for the inhibitor increase with increase of temperature and decrease with increase of the inhibitor concentration in the same temperature. The GON had inhibition efficiency reached 96.96% for the 6 ppm concentration at 298 K.

Keywords

Graphene Oxide Derivatives, Corrosion Inhibitors, Carbon Steel Alloy

1. Introduction

Nowadays the nanocompounds are used in wide field of applications due to their ability to do them because of a large number of the functional groups in their chemical structures. One of them is graphene oxide (GO). In recent years, GO nanosheets have drawn special interest in various fields such as supercapacitors, batteries, and photocatalysis etc. The intriguing properties of GO arises from its chemical composition, which consists of graphene sheets with several oxygenated functional moieties attached, such as hydroxyl, carbonyl, carboxyl and epoxyl groups. In this respect, the chemical composition and physico-chemical

properties of GO are attractive towards the application of corrosion resistant properties [1] [2]. The use of inhibitors for the control of corrosion for metals and alloys which are in contact with aggressive environment is an accepted practice. Large numbers of organic compounds were studied to investigate their corrosion inhibition potential. All these studies reveal that organic compounds especially those with N, S and O showed significant inhibition efficiency [3] [4]; inhibitors are added to the acidic solution during the acidizing process to reduce the aggressive corrosive effects of the acid on tubing and casing materials. Inhibitors are widely used for the protection of metals to corrosion in acidic environments. Inhibitors usually protect the metal by adsorbing on the surface and retarding metal corrosion in aggressive media. Therefore, selecting the appropriate inhibitor for a particular metal is very important. Most of the well-known inhibitors are organic compounds containing nitrogen, and oxygen [5]. A considerable number of studies have been published on the inhibition of steel and its alloys in acidic medium [6] [7] [8] [9] [10].

2. Materials and Method

2.1. Materials

C-steel (C1010) was obtained from Metal Samples (USA) was used with the following composition by percentage weight: C = 0.13, Mn = 0.3, Si = 0.37, P = 0.04, S = 0.05, Cr = 0.1, Ni = 0.3, Cu = 0.3, AS = 0.08 and the remainder is Fe. Ethanol amine, graphite, Hydrogen peroxide, Potassium permanganate, Sodium nitrate, maracapto ethanol from Fluka, Hydrochloric acid, Sulphuric acid from BDH.

2.2. Experimental Methods

2.2.1. Graphene Oxide (GO)

Graphene oxide was synthesized by Hummers method Graphite flakes (2 g) and $NaNO_3$ (2 g) were mixed in 50 mL of H_2SO_4 (98%) in a 1000 mL volumetric flask kept under at ice bath (0˚C - 5˚C) with continuous stirring. The mixture was stirred for 2 hrs at this temperature and potassium permanganate (6 g) was added to the suspension very slowly. The rate of addition was carefully controlled to keep the reaction temperature lower than 15˚C. The ice bath was then removed, and the mixture was stirred at 35˚C until it became pasty brownish and kept under stirring for one days. It is then diluted with slow addition of 100 ml water. The reaction temperature was rapidly increased to 98˚C with effervescence, and the color changed to brown color, Further this solution was diluted by adding additional 200 ml of water stirred continuously for purification. The solution is finally treated with 10 ml H_2O_2 to terminate the reaction by appearance of yellow color, the mixture was washed by rinsing and centrifugation with 10% HCl and then deionized (DI) water several times After filtration and drying under vacuum at room temperature (**Scheme (1-1)**) [11] [12] [13].

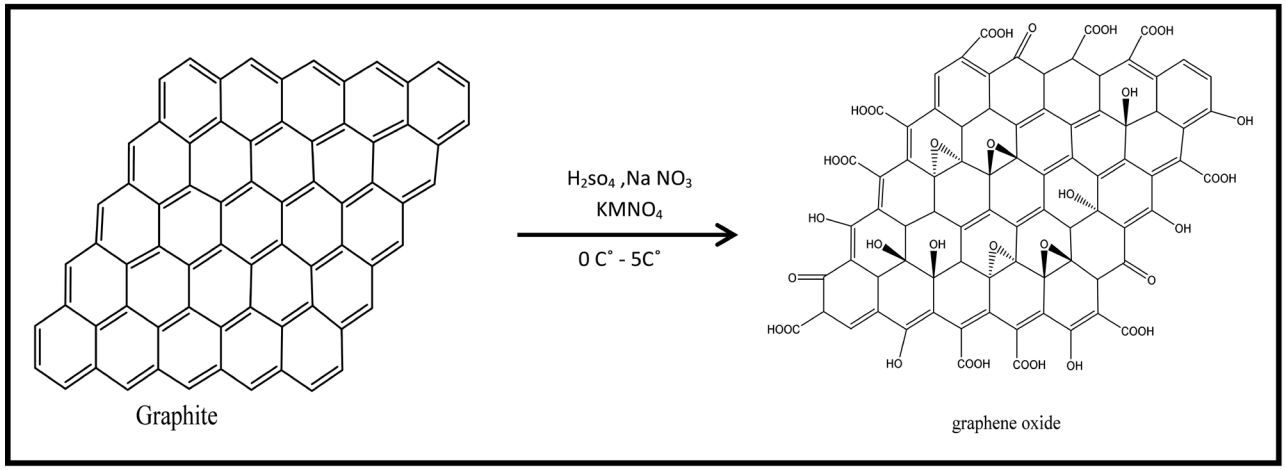

Scheme (1-1). Chemical equation of preparation of GO.

2.2.2. 2-Amino Ethanol and Graphene Oxide Functionalized (GON)

The functionalize GO, (0.5 g) was placed in a (250 mL) dried beaker with (100 mL) DMF and amino ethanol 6.17 mL, 10 mmole) sonicated for 1 h to form homogeneous solution, then added DCC (2.06 g, 10 mmole), DMAP (1.22 g, 10 mmole) into mixture with stir 24 h at room temperature, after the reaction finish, the product was filter, then black powder was dried [14] the preparation process of (GON) is shown in **Scheme (2-2)**.

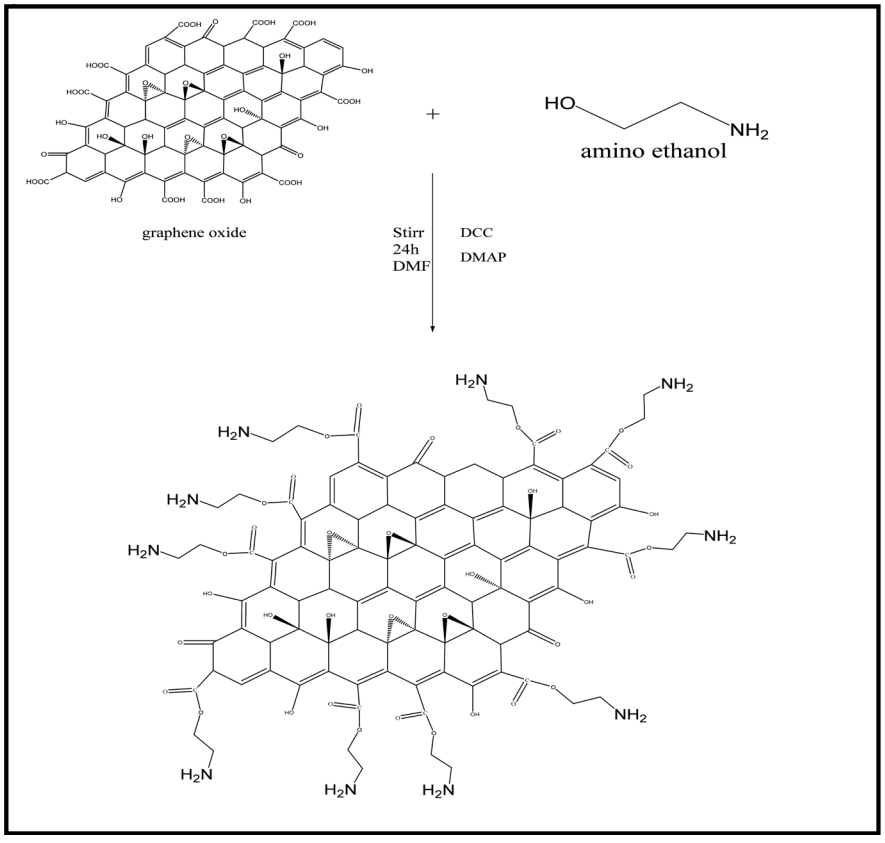

Scheme (2-2). Chemical equation of preparation (GON).

2.2.3. 2-Mercapto Ethanol and Graphene Oxide Functionalized (GOS)

The functionalize GO, (0.5 g) was placed in a (250 mL) dried beaker with (100 mL) DMF and amino ethanol (0.86 mL, 10 mmole) sonicated for 1 h to form homogeneous solution, then added DCC (2.06 g, 10 mmole), DMAP (1.22 g, 10 mmole) into mixture with stir 24 h at room temperature, after the reaction finish, the product was filter, then black powder was dried [14]. The preparation process of (GOS) is shown in **Scheme (2-3)**.

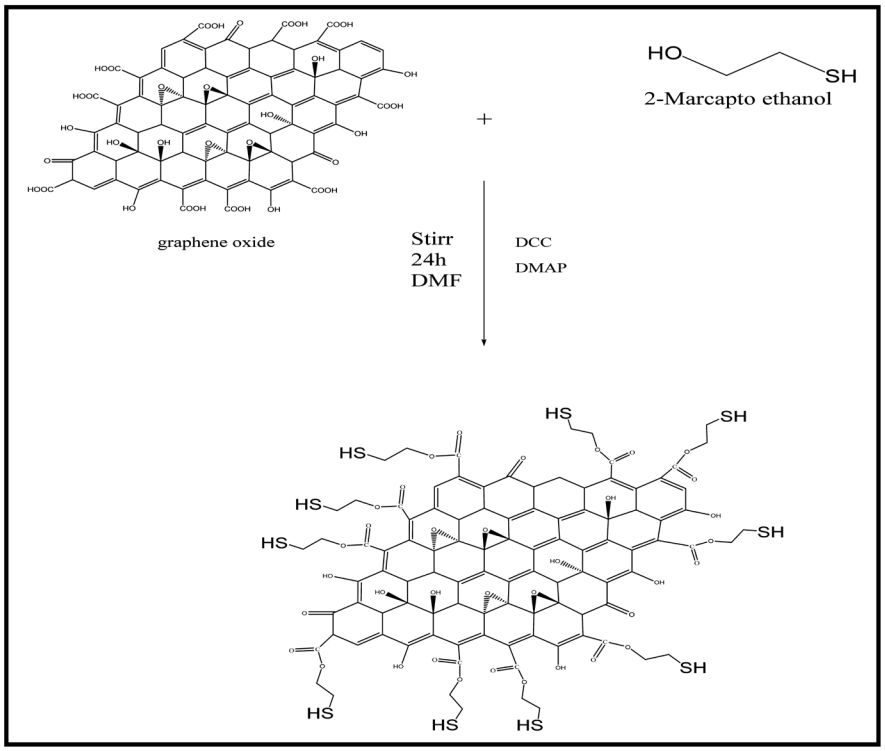

Scheme (2-3). Chemical equation of preparation (GOS).

2.2.4. Electrochemical Measurements

The electrochemical measurements were performed using a potentiostat/galvanostat (ACM) connected to a computer. A three electrode cell assembly, consisting of a C-steel rod embedded in araldite as the working electrode (WE), and a saturated calomel electrode as the reference electrode (RE), aplatinum sheet as the counter electrode (CE), was used for the electrochemical measurements. The temperature of the electrolyte was maintained at the required temperature using a water bath. Before immersion in the test solutions, the WE was polished with a polishing machine using emery paper from 600 to 1200 grade until a mirror image was obtained. Then, the WE was washed with distilled water thenimmersed in acetone for 1Minute in an ultrasonic cleaner. The WE electrode was prepared directly before electrochemical measurements then immersed in the test solution at open circuit potential for one hour until a steady state potential was obtained polarization measurements were performed. All experiments were performed in aerated solutions. From the pola-

rization data, were calculated like the degree of surface coverage (θ), the percent tage inhibition efficiency (% IE), corrosion rate and charge transfer resistance [15].

3. Results and Discussion

3.1. FTIR Spectroscopy Analysis of GO, GON and GOS

FTIR analysis was used to identify functional groups present in the GO, GON_1 and GOS_1. **Figures 1(a)-(c)** shows the FTIR spectrum of, GO, GON_1 and GOS_1 powders respectively, the GO spectrum shows the peak at 3386.39 cm^{-1} due to O-H stretching vibration, 1724.36 cm^{-1} was strong C=O stretching band, and peak at 16,228 cm^{-1}, 1378.85 cm^{-1} can be attributed to C=C stretching of aromatic ring, C-OH bending respectively, the charactestic peak at 1029.8 cm^{-1} due to C-O epoxy group [16] (**Figure 1(b)**). In the spectrum of GON the peak at 3434.6 cm^{-1} for stretching OH groups. The presence of absorption bands at 3334, 3222 cm^{-1} ($-NH_2$) stretching vibration, the peaks 2956, 2823 cm^{-1} assigned to the asymmetric and symmetric stretching of C-H bands, 1639.2 cm^{-1} due to C=O aster stretching vibration, the peak at 1559.17, 1122,37 cm^{-1} attributed to C=C aromatic ring, and C-N stretching, also 1029.8 cm^{-1} due to C-O epoxy group, the peak at 797.421 cm^{-1} due to aromatic C-H bending [17] (**Figure 1(c)**), GOS the peak at 3427.85 cm^{-1} for stretching OH groups. The peaks 2998, 2898 cm^{-1} assigned to the asymmetric and symmetric stretching of $-CH_2$ bands, also S-H band at 2550 cm^{1}, 1648.84 cm^{-1} due to C=O aster stretching vibration, the peak at 1559.77 is attributed to C=C aromatic ring, a, also 1113.69, 1024.02, 620.966 cm^{-1} due to C-O, epoxy, C-S bending [17].

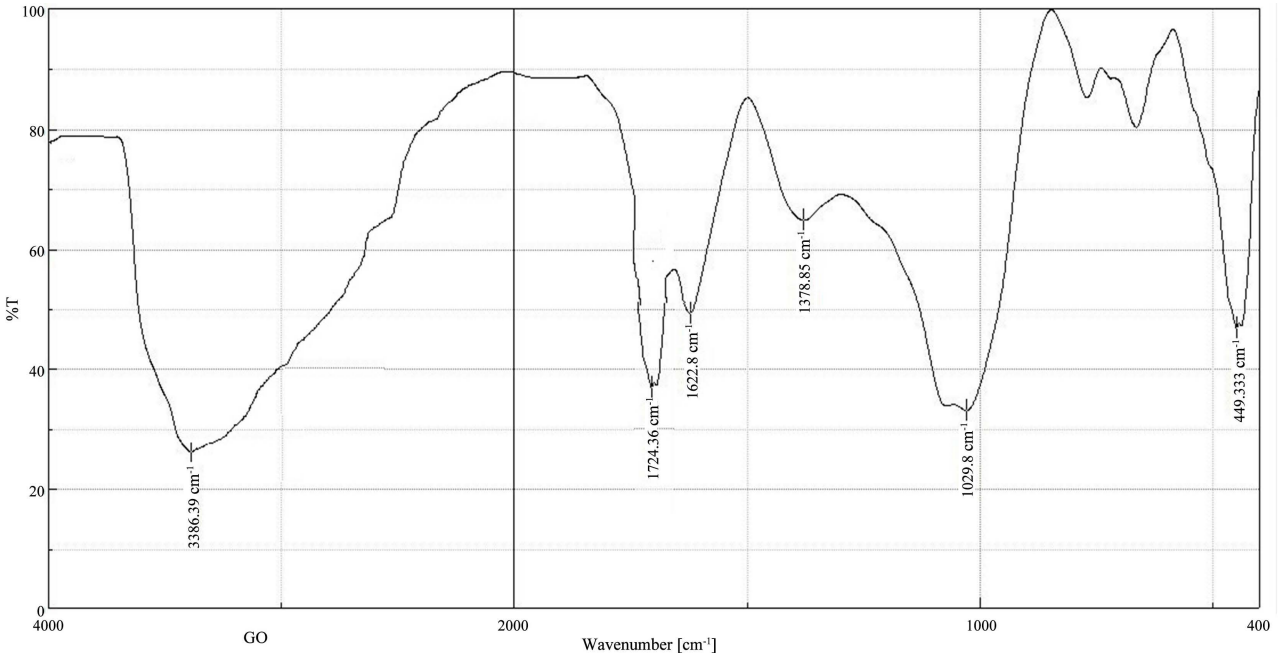

(a)

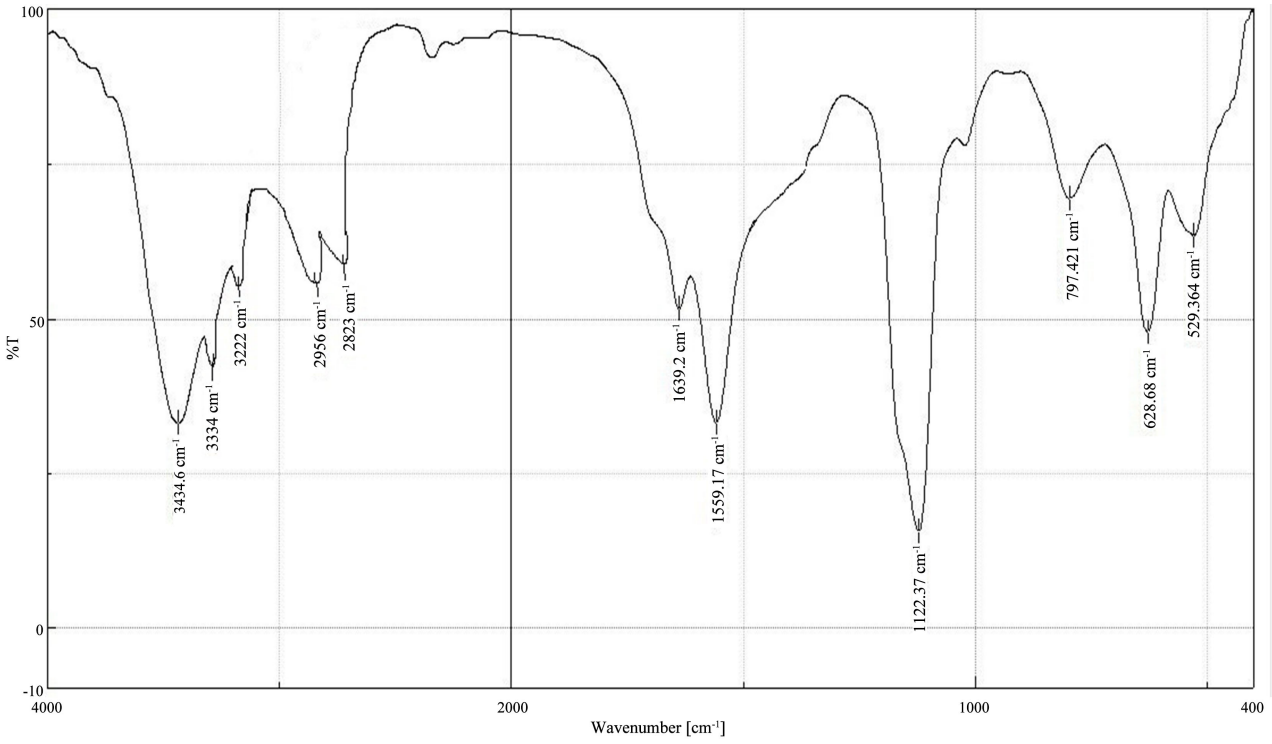

(b)

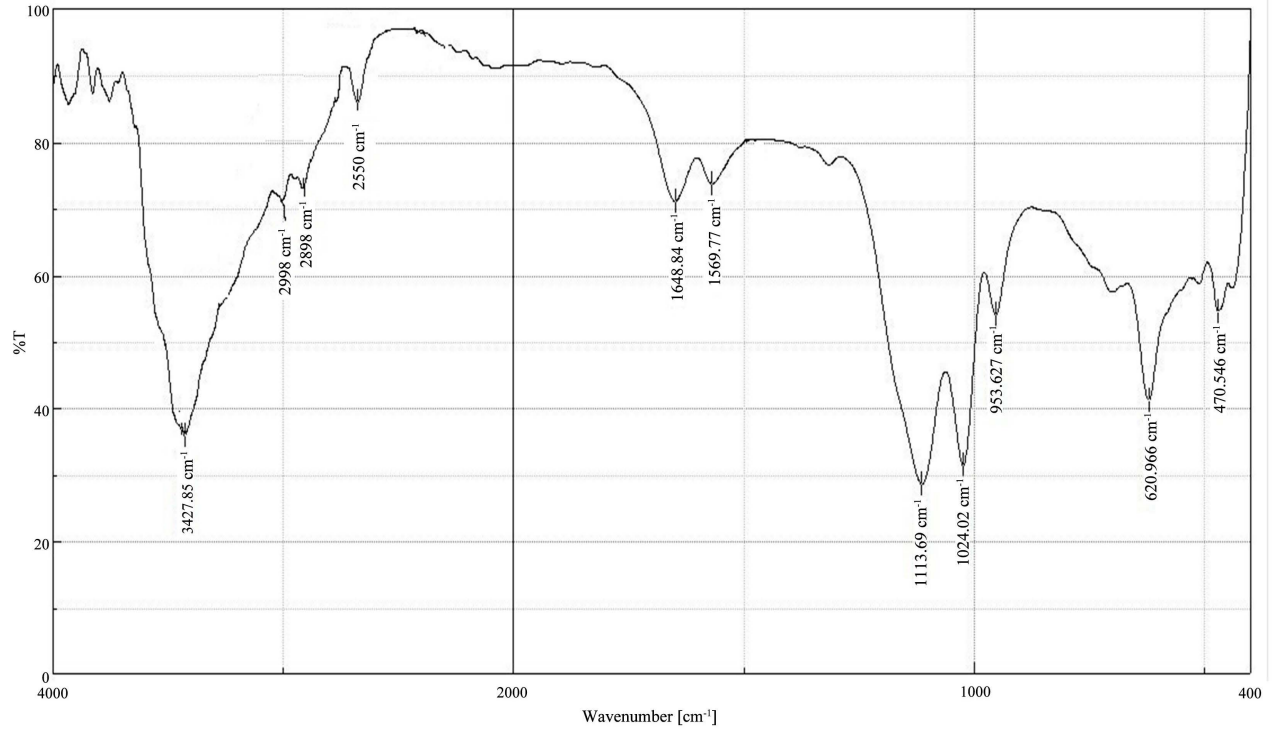

(c)

Figure 1. FTIR spectrum of (a) GO powder; (b) GON powder; (c) GOS powder.

3.2. X-Ray Diffraction (XDR) of GO, GON and GOS

In **Figure 2(a)** the X-Ray Diffraction (XRD) of grapheme oxide shows a large

interlayer spacing equal to 8.06 A˚ at the position (2θ = 10.97˚) disappearance of the peak at 26˚ due to completely oxidized after the chemical oxidation and exfoliation [13] (**Figure 2(b)**), GON shows many peaks appear (2θ = 10.97) at d-spacing 8.06 indicate to graphene oxide and other peaks 2θ = 34.05, 38.80, 54, 72, 55.35, 58.43, 62.15, 65.24, 67.64, 71.28, 72.55 and 73.03 have to d-spacing 2.63, 2.32, 1.67, 1.65, 1.57, 1.49, 1.43, 1.38. 1.30 and 1.29, respectively attributed to functionalized ethanol amine at graphene oxide also intermediate layer [17], (**Figure 2(c)**) of GOS show many peaks appear (2θ = 10.97) at d-spacing 8.06 indicate to graphene oxide and other peaks 2θ = 32.31, 34.05, 38.80, 40.94, 47.47, 48.96, 49, 61, 50.85, 55.47, 59.61, 62.08, 65.29 and 67.63 have to d-spacing 2.77, 2.63, 2.32, 2.20, 1.91, 1.66, 1.83, 1.79. 1.60, 1.55, 1.49, 1.42 and 1.38, respectively attributed to functionalized 2-marcapto ethanol at graphene oxide also intermediate layer [17].

The Diffraction patterns of X-ray to prepared organic compound particles size is calculated using (Debye-Scherer) Equation [18]

$$D = \frac{K\lambda}{\beta COS_{\theta}} \tag{1}$$

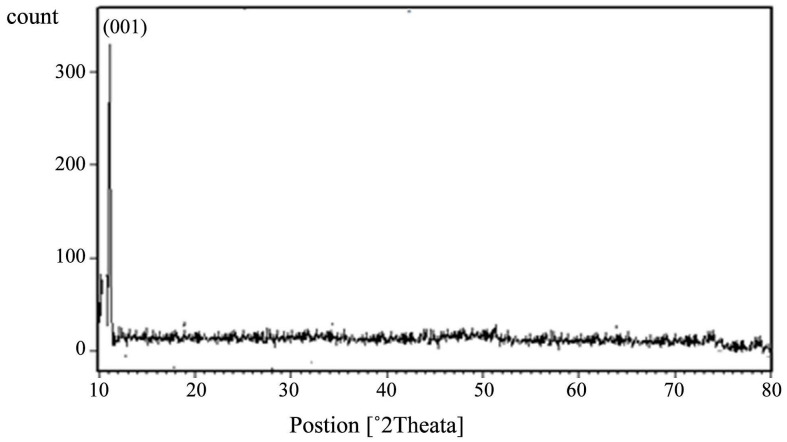

(a)

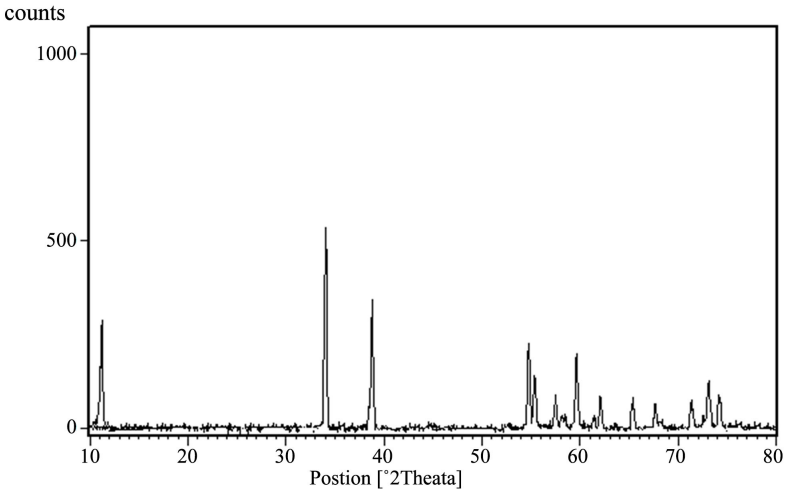

(b)

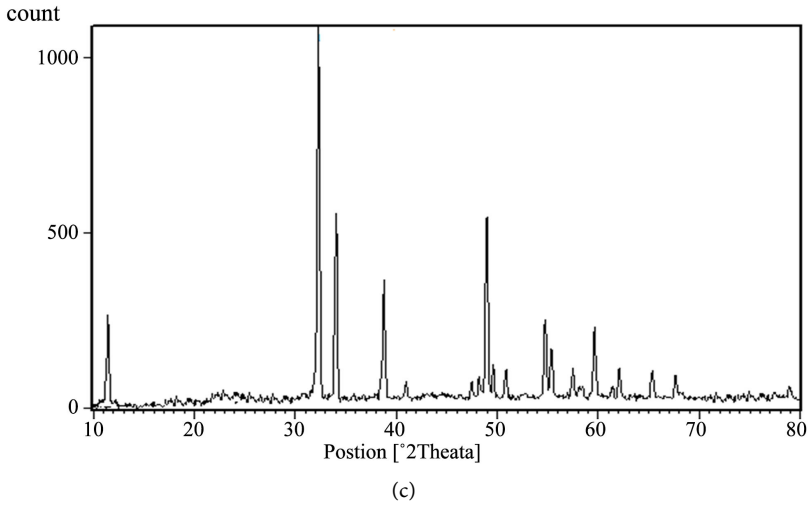

Figure 2. XRD OF (a) GO, (b) GON, (c) GOS.

where; D: Particles size, λ: X-ray wave length (nm), β: Half width at half maximum (HWHM), K: is s related hape factor, normally taken as 0.9. θ is x-ray angle. From this equation the particle size of grapheme oxide (GO) (16 nm) but to calculated average particle size to prepared organic compounds GON (35.7 nm), GOS (36.11 nm), Also calculatedparticles size using (Williamson-Hall) (W-H) equation [19]

$$\beta * \cos\theta = \left[\frac{k\lambda}{D}\right] + \left[4£ + Sin\theta\right] \quad (2)$$

where $£$ micro strain of particles, the calculated particles size from graphic between $(Sin\theta)$ on x-axis, $(\beta * \cos\theta)$ on y-axis, D calculated by intercept ($K\lambda/D$), **Figure 3(a)**, from this equation particles size of GON (17.74 nm), micro strain (−0.00195), (b) GOS (14.26 nm) micro strain (−0.00246).

3.3. Field Emission Scanning Electron Microscopy (FESEM)

The FESEM of graphene oxide (GO) very sharp edges and flat surface the dark gray areas consist of several layers of sheets also kinked and wrinkled areas [13], shown in **Figure 4(a)** but GON observed very thin (3.07 nm) and re-stacked sheets (**Figure 4(b)**), GOSthe re-stacked layers and crumpling, kinked and wrinkled areas [20] [21] (**Figure 4(c)**).

3.4. Electrochemical Measurements

3.4.1. Polarization Measurements (Tafel Method)

Typical potentiodynamic polarization curves for the C-steel in 1M HCl in the presence and absence of different concentrations of GO, GON, GOS are shown in (**Figures 5-16**). The respective Tafel parameters, inhibition efficiency (% IE), I_{corr} corrosion current, corrosion rate and charge transfer resistance are provided in **Tables 1-3**. It is clear that the shapes of the Tafel plots for the inhibited electrodes are different from those of uninhibited electrodes. The presence of the in-

hibitor decreases the current density but does not change other aspects of the behavior.

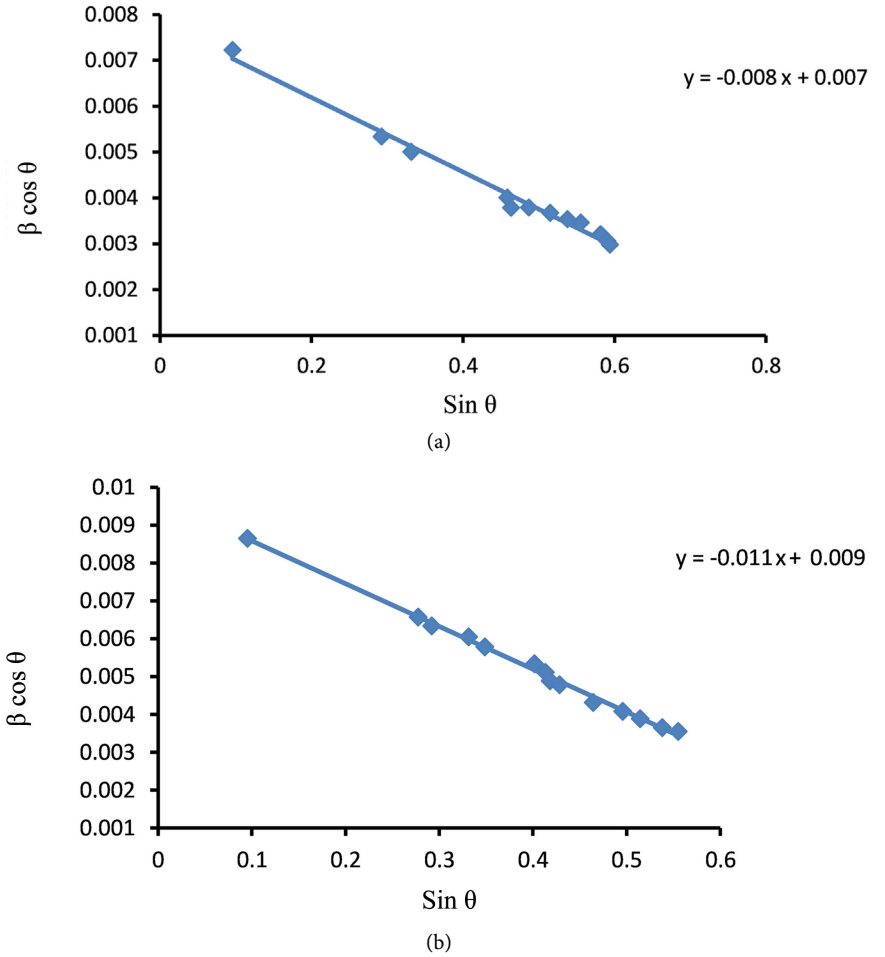

Figure 3. Scheme Williamson-Hall to (a) GON, (b) GOS.

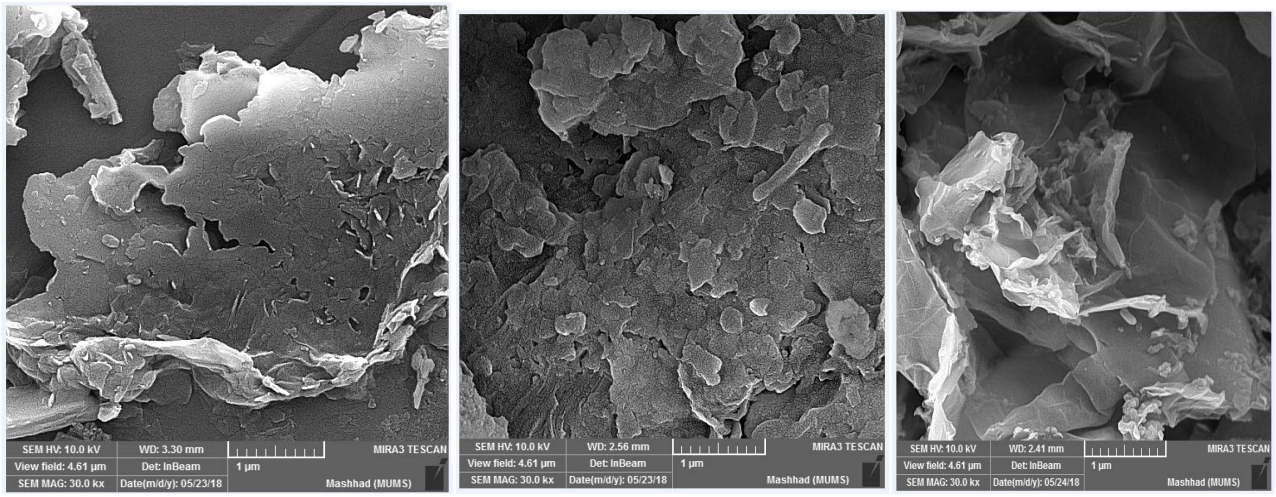

(a) (b) (c)

Figure 4. FESEM OF (a) GO, (b) GON, (c) GOS.

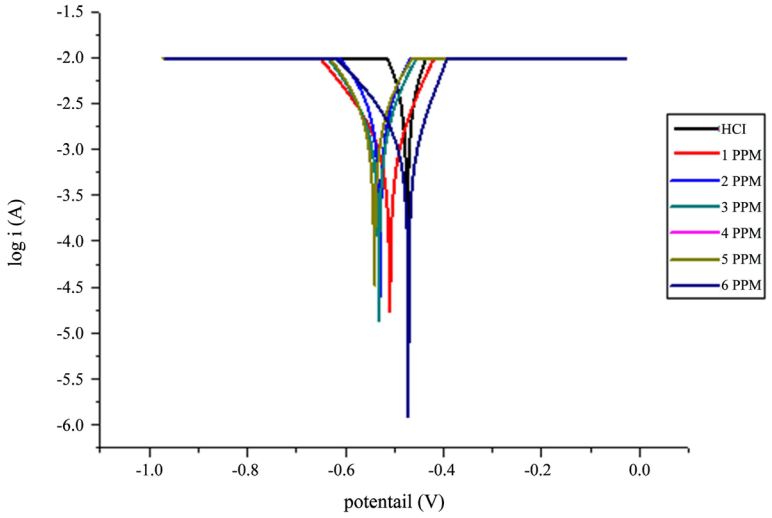

Figure 5. Tafel Plot of GOt concentration (1 - 6 ppm) on C-steel alloy in 298 k.

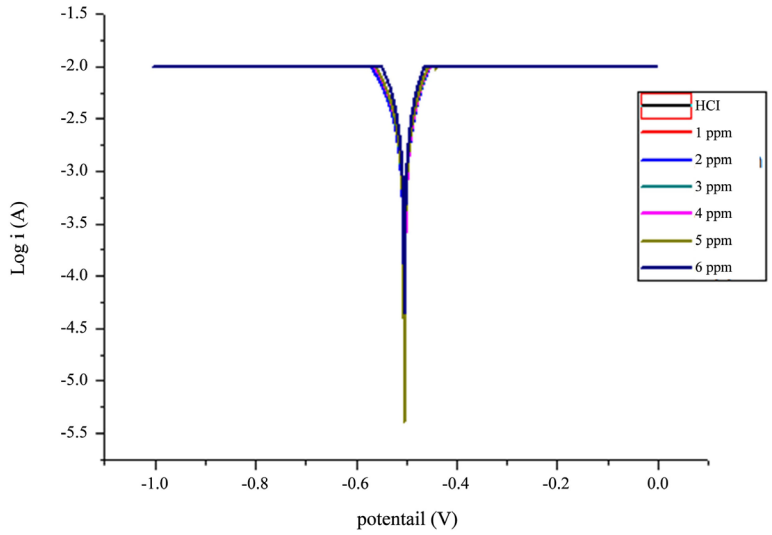

Figure 6. Tafel Plot of GO concentration (1 - 6 ppm) on C-steel alloy in 308 k.

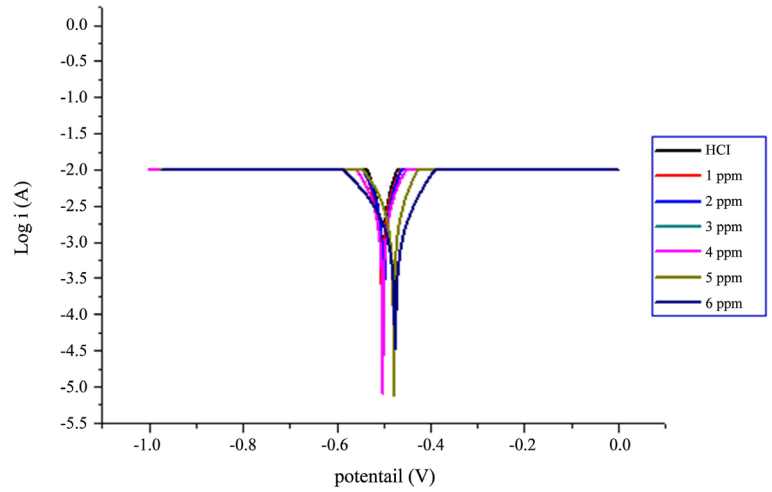

Figure 7. Tafel Plot of GO concentration (1 - 6 ppm) on C-steel alloy in 318 k.

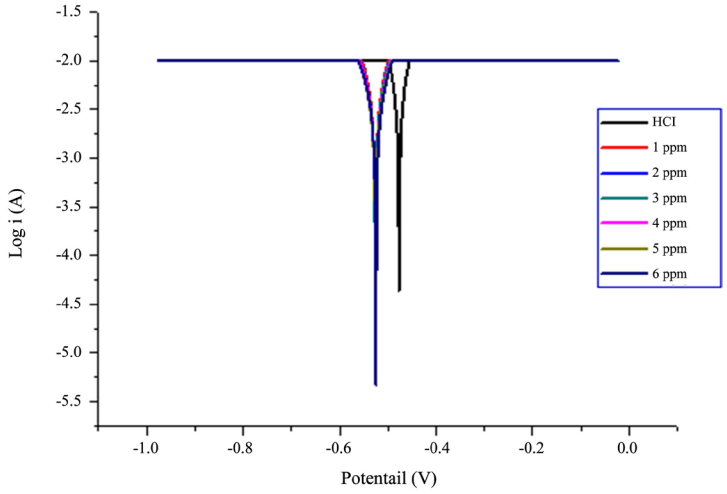

Figure 8. Tafel Plot of GO concentration (1 - 6 ppm) on C-steel alloy in 328 k.

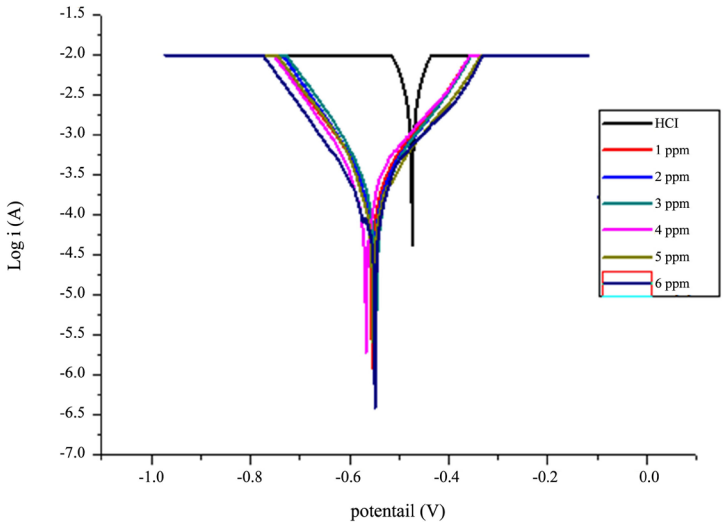

Figure 9. Tafel Plot of GON concentration (1 - 6 ppm) on C-steel alloy in 298 k.

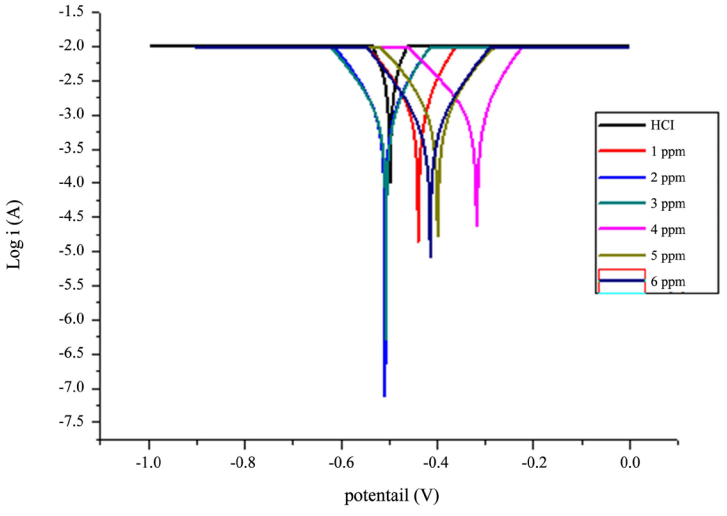

Figure 10. Tafel Plot of GON concentration (1 - 6 ppm) on C-steel alloy in 308 k.

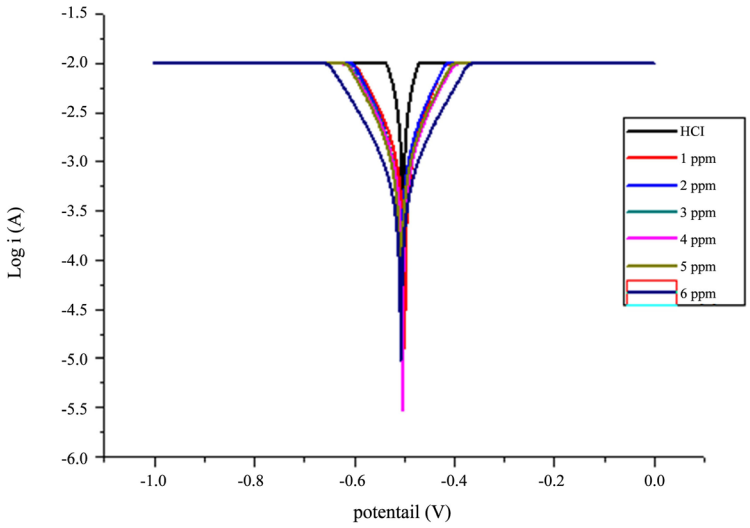

Figure 11. Tafel Plot of GON concentration (1 - 6 ppm) on C-steel alloy in 318 k.

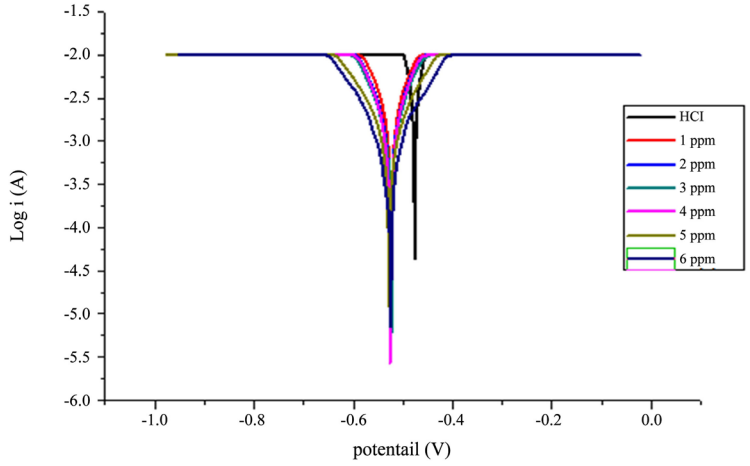

Figure 12. Tafel Plot of GON concentration (1 - 6 ppm) on C-steel alloy in 328 k.

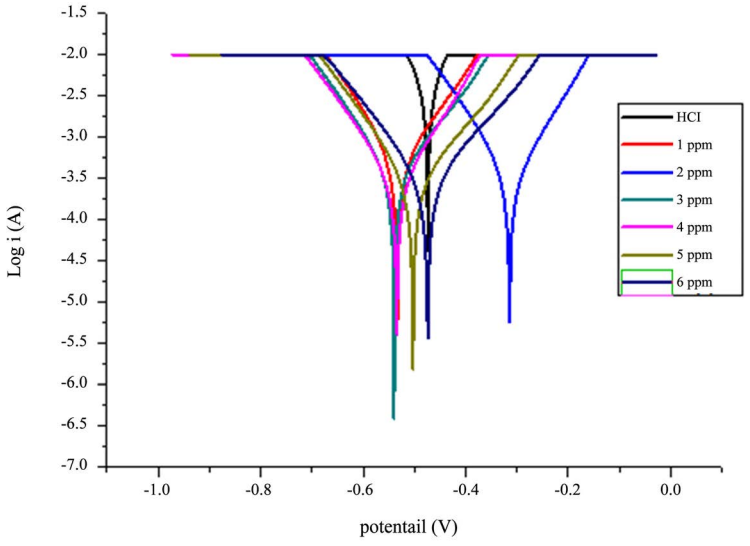

Figure 13. Tafel Plot of GOS concentration (1 - 6 ppm) on C-steel alloy in 298 k.

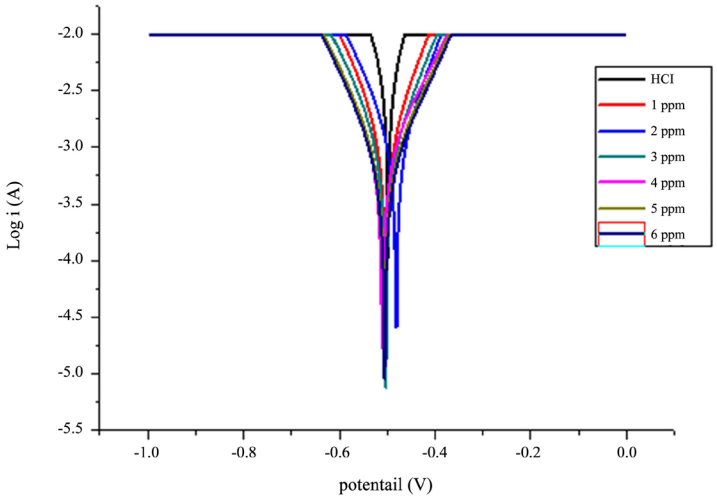

Figure 14. Tafel Plot of GOS concentration (1 - 6 ppm) on C-steel alloy in 308 k.

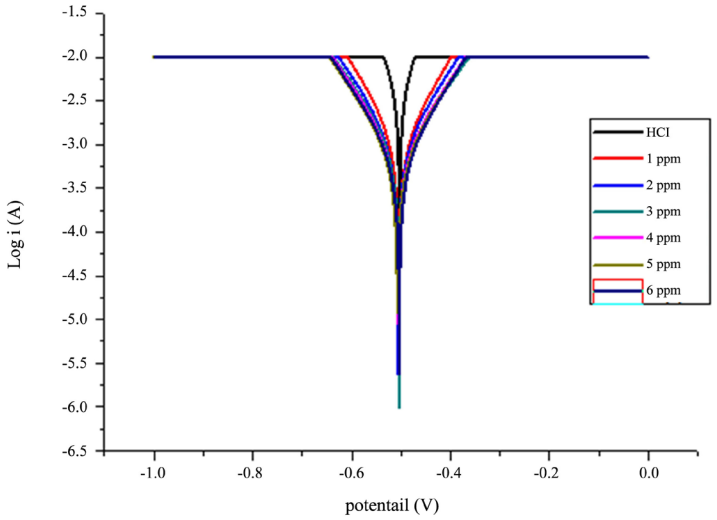

Figure 15. Tafel Plot of GOS concentration (1 - 6 ppm) on C-steel alloy in 318 k.

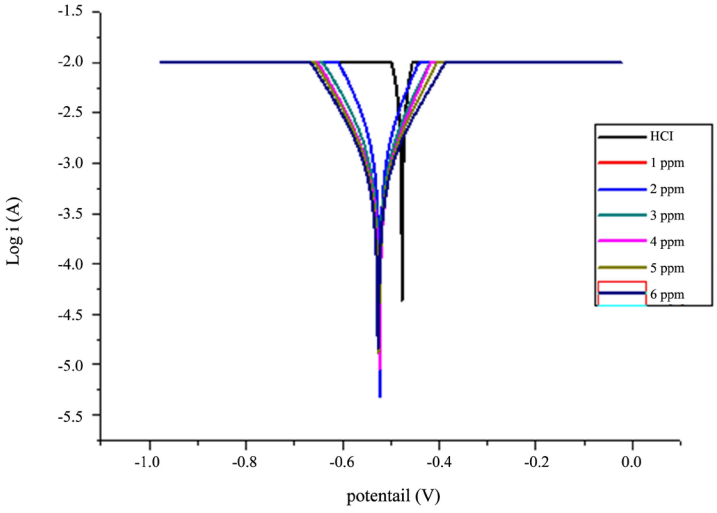

Figure 16. Tafel Plot of GOS concentration (1 - 6 ppm) on C-steel alloy in 328 k.

Table 1. Tafel parameters for C-steel 1M HCl in the absence and presence of different concentrations of GO at different Temp.

Comp.	Temp(K)	I_{corr} ($\mu A \cdot Cm^{-2}$)	CR (mpy)	R_{ct} (Ω)	E_{corr} (mV)	βa (mV/de.)	$-\beta c$ (mV/de.)	Eff.%
HCl	298	726.98	337.12	41.82	−474	16.47	−8.233	-
1 ppm		318.22	147.56	95.54	−511	12.00	−7.360	56.22
2 ppm		287.22	133.2	105.9	−514	4.887	−7.428	60.48
3 ppm		234.20	108.60	129.8	−510	8.046	−7.212	67.78
4 ppm		195.86	90.84	155.2	−502	8.668	−7.422	73.05
5 ppm		153.25	71.04	198.4	−474	9.502	−6.992	78.92
6 ppm		138.70	64.32	219.2	−494	11.45	−7.621	80.92
HCl	308	801.07	371.44	37.96	−498	9.312	−8.233	–
1 ppm		692.07	252.36	43.94	−496	5.460	−5.183	32.05
2 ppm		544.26	245.44	55.87	−507	4.321	−9.522	33.92
3 ppm		529.35	239.96	58.75	−503	8.551	−1.647	35.39
4 ppm		517.51	217.16	57.45	−504	4.059	−4.335	41.53
5 ppm		467.22	211.28	64.93	−505	10.86	−8.097	43.11
6 ppm		455.74	205. 6	66.93	−505	3.352	−1.647	44.64
HCl	318	927.81	430.4	32.77	−504	4.117	−1.647	-
1 ppm		719.17	333.48	42.28	−506	12.34	−1.647	22.51
2 ppm		700.71	324.88	43.40	−499	8.233	−1.647	49.03
3 ppm		658.22	305.2	46.20	−506	4.231	−1.647	29.08
4 ppm		516.45	239.48	58.55	−506	4.219	−1.647	44.35
5 ppm		442.13	205	68.77	−491	8.233	−7.207	52.36
6 ppm		210.06	97.4	74.48	−490	8.851	−7.464	77.36
HCl	328	1396.45	647.6	21.77	−477	16.47	−8.233	-
1 ppm		1115.03	517.2	27.27	−523	16.47	−1.647	20.13
2 ppm		1032.43	479.6	29.39	−522	8.233	−1.647	25.94
3 ppm		1008.99	446.8	30.13	−524	8.233	−1.647	31.00
4 pmm		953.14	442	31.90	−515	8.233	−1.647	31.74
5 ppm		871.48	400.32	36.98	−503	8.233	−1.647	38.18
6 ppm		840.95	389.92	39.16	−525	8.233	−1.647	39.79

Table 2. Tafel parameters for C-steel 1M HCl in the absence and presence of different concentrations of GON at different Temp.

Comp.	Temp (K)	I_{corr} ($\mu A \cdot Cm^{-2}$)	CR (mpy)	R_{ct} (Ω)	E_{corr} (mV)	βa (mV/de.)	$-\beta c$ (mV/de.)	Eff.%
HCl	298	726.98	337.12	41.82	−474	16.47	−8.233	–
1 ppm		32.97	15.28	92.23	−490	7.885	−8.680	95.46
2 ppm		29.54	13.70	102.9	−496	7.449	−9.793	95.93
3 ppm		28.84	13.37	105.4	−481	8.276	−11.018	96.03

Continued

4 ppm		27.23	12.58	111.7	−499	7.027	−9.075	96.26
5 ppm		25.50	11.82	119.2	−488	8.807	−9.314	96.49
6 ppm		22.11	10.22	137.9	−482	6.658	−9.721	96.96
HCl		801.07	371.44	37.96	−498	9.312	−8.233	-
1 ppm		188.76	87.52	161.1	−459	6.660	−9.039	76.43
2 ppm		153.49	71.20	198.0	−532	10.57	−9.814	80.83
3 ppm	308	148.76	68.96	204.5	−524	10.76	−9.371	81.43
4 ppm		142.72	66.20	213.0	−414	10.13	−7.539	82.17
5 ppm		128.52	59.60	236.6	−448	9.286	−8.969	83.95
6 ppm		84.09	38.992	361.6	−418	10.24	−9.676	89.50
HCl		927.81	430.4	32.77	−504	4.117	−1.647	-
1 ppm		188.64	87.48	162.1	−520	8.209	−9.489	79.67
2 ppm		187.22	86.80	162.4	−530	10.14	−9.701	79.83
3 ppm	318	161.78	75.48	186.8	−526	9.312	−9.078	82.46
4 ppm		160.12	74.24	189.9	−522	9.431	−9.059	82.75
5 ppm		150.41	69.76	202.1	−528	9.369	−9.610	83.79
6 ppm		81.62	37.84	372.5	−516	9.473	−9.171	91.20
HCl		1396.45	647.6	21.77	−477	16.47	−8.233	-
1 ppm		451.24	209.28	67.3	−500	2.720	−1.727	67.68
2 ppm		352.07	163.24	86.8	−507	5.448	−1.563	74.79
3 ppm	328	312.90	144.84	97.1	−501	2.204	−4.590	77.63
4 ppm		266.04	121.36	114.3	−503	8.827	−2.043	81.26
5 pmm		189.70	89.48	157.6	−492	9.529	−8.213	86.18
6 ppm		113.15	52.48	268.7	−493	9.509	−8.415	91.89

Table 3. Tafel parameters for C-steel 1M HCl in the absence and presence of different concentrations of GOS at different Temp.

Comp.	Temp (K)	I_{corr} ($\mu A \cdot Cm^{-2}$)	CR (mpy)	R_{ct} (Ω)	E_{corr} (mV)	βa (mV/de.)	$-\beta c$ (mV/de.)	Eff.%
HCl		726.98	337.12	41.82	−474	16.47	−8.233	–
1 ppm		65.07	30.168	54.96	−509	8.586	−1.003	91.05
2 ppm		45.89	21.28	66.25	−291	10.24	−9.752	93.68
3 ppm	298	43.31	20.11	70.19	−518	7.881	−9.763	94.03
4 ppm		37.83	17.54	80.38	−508	9.645	−9.297	94.79
5 ppm		31.85	14.76	95.49	−520	7.507	−9.526	95.62
6 ppm		27.05	14.18	99.37	−522	7.444	−8.909	95.79
HCl		801.07	371.44	37.96	−498	9.312	−8.233	-
1 ppm	308	168.17	77.96	180.8	−510	11.12	−9.724	79.01

Continued

2 ppm		149.35	69.28	203.5	−489	11.36	−9.865	81.34
3 ppm		121.42	56.32	250.4	−509	10.96	−9.655	84.83
4 ppm		104.79	48.6	290.2	−512	8.623	−9.297	86.91
5 ppm		90.84	42.12	334.7	−504	9.171	−9.728	88.66
6 ppm		80.73	37.43	376.7	−506	9.214	−9.881	89.92
HCl		927.81	430.4	32.77	−504	4.117	−1.647	-
1 ppm		144.26	66.88	210.8	−511	10.12	−9.816	84.46
2 ppm		114.77	53.24	264.6	−508	9.386	−9.406	87.63
3 ppm	318	96.12	44.56	316.3	−511	8.697	−9.121	89.64
4 ppm		93.20	43.20	326.3	−512	9.024	−9.278	89.96
5 ppm		83.25	38.60	365.2	−511	9.400	−9.390	91.03
6 ppm		82.37	38.19	369.1	−504	9.682	−9.408	91.12
HCl		1396.45	647.6	21.77	−477	16.47	−8.233	-
1 ppm		497.28	230.60	61.12	−533	8.233	−1.647	64.39
2 ppm		226.86	105.20	134.0	−516	7.887	−9.017	83.75
3 ppm	328	145.92	67.12	210.1	−517	10.13	−9.004	89.63
4 ppm		115.14	53.40	264.1	−520	10.92	−9.176	91.75
5 pmm		108.93	50.52	279.1	−519	9.679	−8.829	92.19
6 ppm		94.52	43.84	321.7	−526	8.197	−8.771	93.23

It is evident from **Tables 1-3** from E_{corr} at constant temperature compared with E_{corr} to blank at 298 K for graphene oxide (GO) the E_{corr} decrease at all concentration compared with E_{corr} to blank that value (−474 mv) but this decreasing less to (89 mv) so inhibitor behavior it mix inhibitor, as observed from previous studies [22] [23] [24], if the difference E_{corr} between blank and inhibitor (89 mv) decreasing less the inhibitor is mix, also E_{corr} other organic inhibitors GON, GOSdecreasing less (89 mv) compared with E_{corr} blank that mean It behavesmix inhibitor at all concentration (1 - 6 ppm) and temperature (298 - 328 K). In this study used very small concentration organic inhibitors it gives high efficiency inhibitor, show graphene oxide have less efficiency inhibitor (20.13%) at (1 ppm) and (80.92%) at (6 ppm) in spite of containing carboxylic group in graphene oxide layer GON, GOS have efficiency inhibitor (67.68%, 64.39%), respectively at (1 ppm) and (96.96%, 95.79%) respectively at (6 ppm) at different temperature.

The R_{ct} values of the inhibited are increase as the concentration of the inhibitors increases on the other hand increase in efficiency inhibitors due to productive carbon steel surface to resist polarization, and the anodic reaction the dissolution of Iron in carbon steel alloy to reduce in present inhibitors the signification that increase of Tafel (β_a) [25].

3.4.2. Effect of Temperature

The study of effect of temperature on the corrosion rate to the organic inhibtors on carbon steel alloylwere immersed in 1 M hydrochloric acid with different concentration (1 - 6 ppm) of inhibitor at temperature ranging from 298 K, 308 K, 318 K, and 328 K, the activation energy value was calculated from Arrhenius equation [26]

$$\ln \mathrm{CR} = \ln \mathrm{A} - \frac{-\mathrm{Ea}}{\mathrm{RT}} \tag{3}$$

where: CR = corrosion rate (mpy), Ea = activation energy (KJ/mol);

A = frequency factor, R= molar gas constant (8.3143 $\mathrm{J{\cdot}K^{-1}{\cdot}mol^{-1}}$);

T = temperature (K).

Figure 17, Figure 18, Figure 19 show good relationship between (ln CR) vs (1/T $\mathrm{K^{-1}}$) for without and with inhibitors organic compound in 1M HCl solution, straight lines were obtained with slope of (–Ea/R), the activation energy was calculated from slope of Arrhenius plot. the activation energy as the concentration of inhibitor increase which indicates physical adsorption [27] and it due to be corrosion reaction in which charge transfer has been blocked by the adsorption of inhibitor molecular on the carbon steel surface. The activation energy (Ea) value in the presence of corrosion inhibitors is higher than in absence of inhibitor also Ea increase with increasing concentration in inhibitors.

Enthalpy (ΔH) and entropy (ΔS) of activation have been calculated from the following equation

$$\mathrm{CR} = \frac{\mathrm{RT}}{\mathrm{Nh}} Ln\left(\frac{\Delta \mathrm{S}^*}{\mathrm{R}}\right) Ln\left(\frac{-\Delta \mathrm{H}^*}{\mathrm{RT}}\right) \tag{4}$$

CR = corrosion rate (mpy), ΔH = Enthalpy (KJ/mol), ΔS = entropy (J/mol, K), R= molar gas constant (8.3143 $\mathrm{J{\cdot}K^{-1}{\cdot}mol^{-1}}$), T= temperature (K), N = Avogadro number (6.022×10^{23} $\mathrm{mol^{-1}}$); h = plank, constant (6.62×10^{-34} J·s).

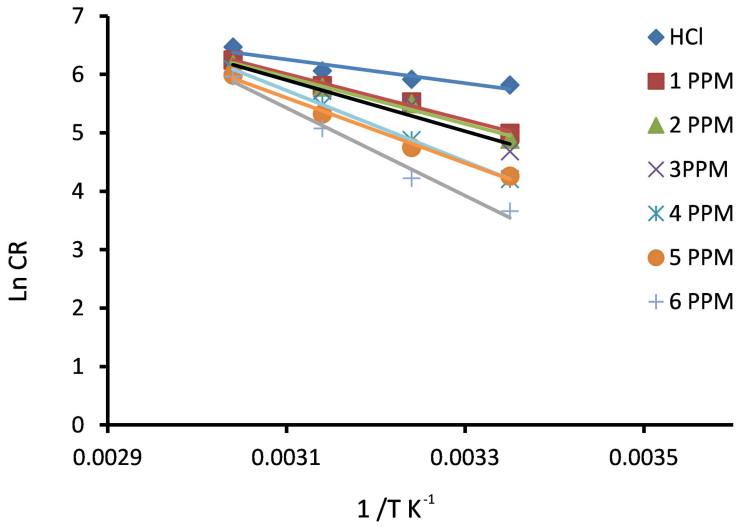

Figure 17. Adsorption isotherm plot for ln (CR) vs 1/T to the GO.

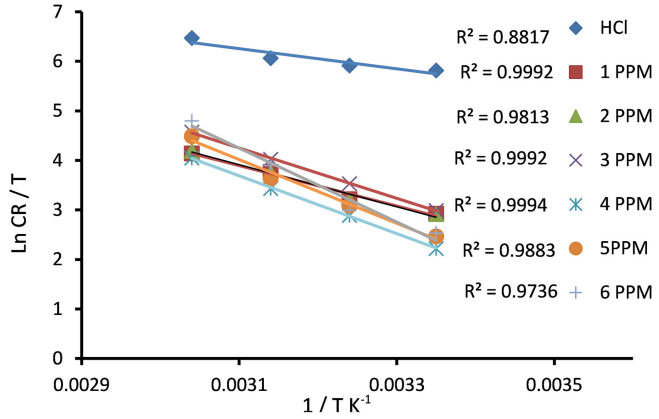

Figure 18. Adsorption isotherm plot for ln (CR) vs 1/T GON.

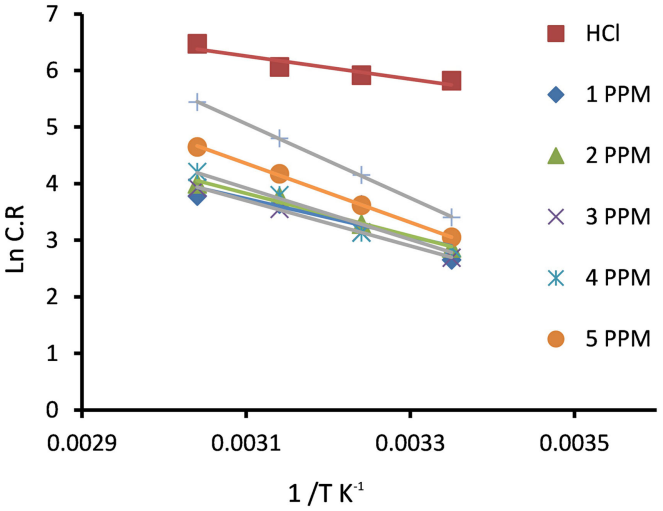

Figure 19. Adsorption isotherm plot for ln (CR) vs 1/T GOS.

Figure 20, **Figure 21**, **Figure 22** are the plots of (ln CR/T) vs (1/T K^{-1}) for carbon steel in with and without inhibitors organic compound in 1N HCl solution. Curves showed straight lines with slope ($\Delta H^*/R$) and intercept ($\Delta S^*/R$). The positive value of ΔH^* reflect that the process of desorption of the inhibitors on the surface is an endothermic process (chemical adsorption) and it has been clearly observed that the value of ΔH^* increasing as the concentration inhibitor increase. The entropy of activation in mentioned table clear that these values increased positively in the presence of inhibitor than in its absence. The increase of reveals that an increase in disordering takes place from reactant to the activated complex [28] (**Tables 4-6**).

3.4.3. Adsorption Isotherm

The adsorption isotherms provide basic information about the interaction between the inhibitor and the Carbon steel surface. In this study fit with Langmuir isotherm and the Langmuir isotherm best model to gives of value of (R^2) correlation coefficient equal one or approaching one, through R^2 to found Langmuir

isotherm was calculated using the equation below [29]

$$\frac{\theta}{1-\theta} = K.C \tag{5}$$

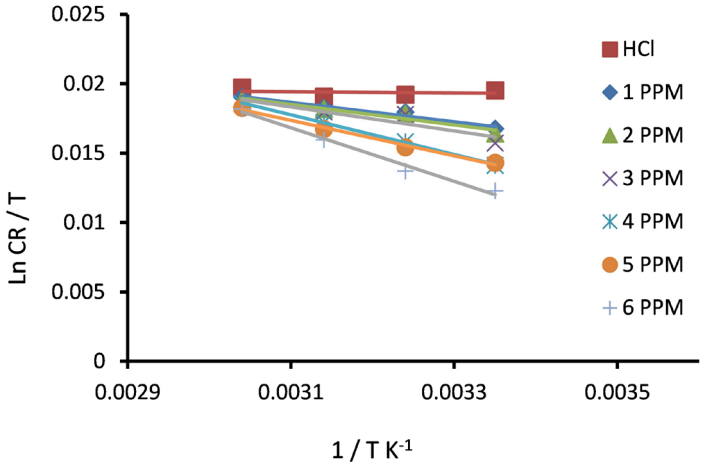

Figure 20. Adsorption isotherm plot for (ln CR/T) vs 1/T to the GO.

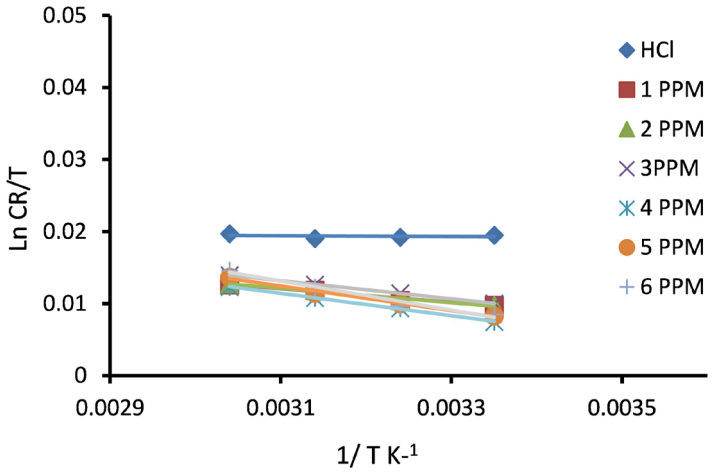

Figure 21. Adsorption isotherm plot for (ln CR/T) vs 1/T GON.

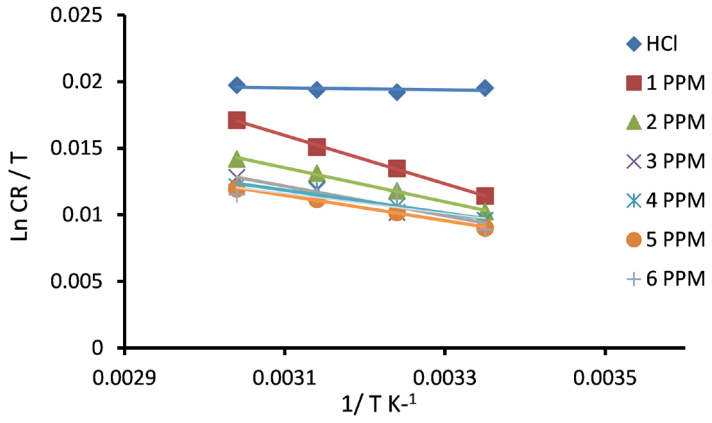

Figure 22. Adsorption isotherm plot for (ln CR/T) vs 1/T GOS.

Table 4. Kinetic parameters Ea*, ΔH*, ΔG* and ΔS* for carbon steel of GO in 1M HCl at (1, 6 ppm).

Conc. (ppm)	Ea* (KJ/mol)	ΔH* (KJ/mol)	Δs* (J/mol·K)	G* (KJ/mol·K)Δ			
				298 K	308 K	318 K	328 K
Blank	17	3.46	17.23	−1.67	−1.84	−2.01	−2.19
1 ppm	33	58.23	33.56	48.23	47.89	47.56	47.22
2 ppm	33	61.21	34.36	50.97	50.62	50.28	49.94
3 ppm	36	71.88	37.52	60.70	60.32	59.95	59.57
4 ppm	50	118.94	51.64	103.55	103.03	102.52	102.00
5 ppm	57	140.93	57.97	123.66	123.08	122.50	121.92
6 ppm	62	160.41	63.72	141.42	140.79	140.15	139.51

Table 5. Kinetic parameters Ea*, ΔH*, ΔG* and ΔS* for carbon steel of GON in 1M HCl at (1, 6 ppm).

Conc. (ppm)	Ea* (KJ/mol)	ΔH* (KJ/mol)	Δs* (J/mol·K)	G*(KJ/mol·K)Δ			
				298 K	308 K	318 K	328 K
Blank	16.88	3.46	17.23	−1.67	−1.84	−2.01	−2.19
1 ppm	33.81	79.15	34.58	68.85	68.50	68.16	67.81
2 ppm	35.34	83.90	36.10	73.15	72.78	72.42	72.06
3 ppm	42.26	104.14	43.25	91.25	90.82	90.39	89.96
4 ppm	48.58	129.71	49.73	114.89	114.40	113.90	113.400
5 ppm	53.41	142.45	54.51	126.20	125.66	125.11	124.57
6 ppm	61.92	168.26	63.10	149.46	148.83	148.20	147.57

Table 6. Kinetic parameters Ea*, ΔH*, ΔG* and ΔS* for carbon steel of GOS in 1M HCl at (1, 6 ppm).

Conc. (ppm)	Ea* (KJ/mol)	ΔH* (KJ/mol)	Δs* (J/mol·K)	G* (KJ/mol·K)Δ			
				298 K	308 K	318 K	328 K
Blank	16.88	3.46	17.23	−1.67	−1.84	−2.01	−2.19
1 ppm	27.75	70.66	31.71	61.21	60.90	60.58	60.26
2 ppm	31.20	71.53	32.05	61.98	61.66	61.34	61.02
3 ppm	33.28	79.26	34.11	69.09	68.75	68.41	68.07
4 ppm	37.75	91.77	38.56	80.28	79.90	79.51	79.12
5 ppm	43.22	106.61	44.28	93.41	92.97	92.53	92.08
6 ppm	54.63	138.44	55.96	121.77	121.21	120.65	120.09

where surface coverage (θ) for various inhibitor concentrations, K_{ads} the adsorptive equilibrium constant, C is the concentration of the inhibitor, the isotherms at different temperatures for different concentration of organic compound in 1M HCl, show date in Tables 7-9 and Figures 23-25.

The equilibrium constant for the adsorption process was related to the standardfree energy of adsorption by the expression [30].

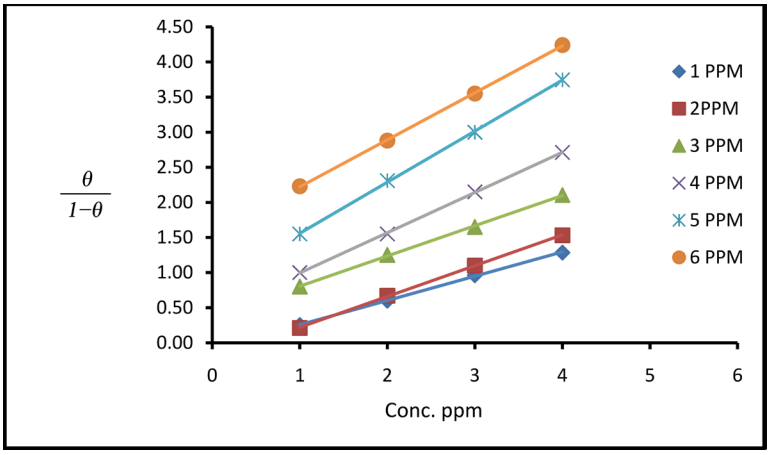

Figure 23. Langmuir s adsorption isotherm plots for the adsorption of GO at different conc. In 1N HCl on carbon steel surface.

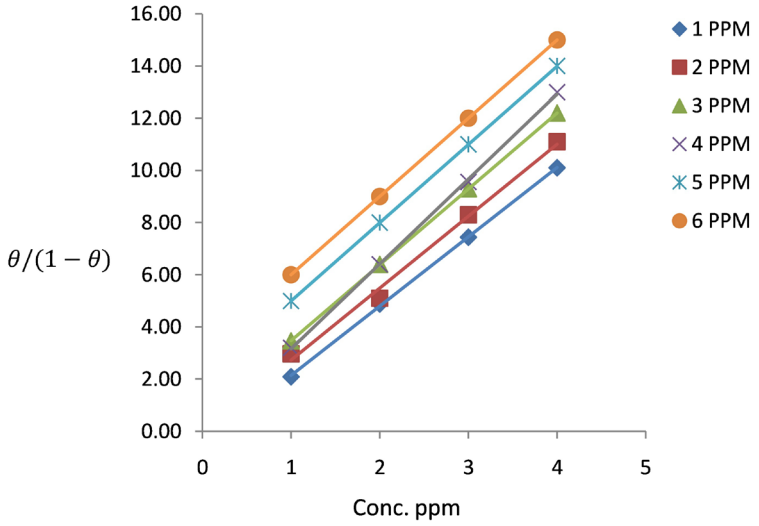

Figure 24. Langmuir s adsorption isotherm plots for the adsorption of GON at different conc. In 1N HCl on carbon steel surface.

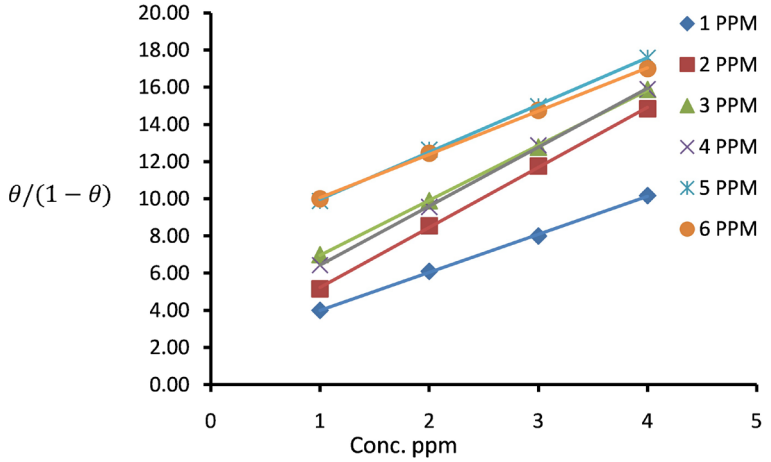

Figure 25. Langmuir s adsorption isotherm plots for the adsorption of GOS at different conc. In 1N HCl on carbon steel surface.

Table 7. Values of ($\theta/1-\theta$), concentration (ppm) and R^2 graphene oxide inhibiter at difference temperatures and (1, 6 ppm) concentration.

CONC. (ppm)	$\theta/1-\theta$				R^2
	298 K	308 K	318 K	328 K	
1	1.28	0.96	0.60	0.25	0.9996
2	1.53	1.10	0.67	0.21	0.9997
3	2.10	1.65	1.25	0.80	0.9994
4	2.71	2.15	1.55	1.00	0.9997
5	3.75	3.00	2.31	1.55	0.9997
6	4.24	3.55	2.88	2.23	0.9998

Table 8. Values of ($\theta/1-\theta$), concentration (ppm) and R^2 GON inhibiter at difference temperatures and (1 - 6 ppm) concentration.

CONC . (ppm)	$\theta/1-\theta$				R^2
	298 K	308 K	318 K	328 K	
1	10.10	7.44	4.88	2.09	0.9997
2	11.10	8.30	5.10	2.97	0.9942
3	12.20	9.30	6.40	3.47	1
4	13.00	9.56	6.40	3.20	0.9996
5	14.00	11.00	8.00	5.00	1
6	15.00	12.00	9.00	6.00	1

Table 9. Values of ($\theta/1-\theta$), concentration (ppm) and R^2 GOS at difference temperatures and (1 - 6 ppm) concentration.

CONC. (ppm)	$\theta/1-\theta$				R^2
	298 K	308 K	318 K	328 K	
1	10.17	8.00	6.10	4.00	0.9994
2	14.84	11.76	8.55	5.16	0.9995
3	15.88	12.78	9.90	7.00	0.9997
4	15.89	12.87	9.55	6.43	0.9997
5	17.59	14.98	12.65	9.89	0.9998
6	17.00	14.76	12.45	10.00	0.9996

$$\Delta G^{\circ}_{ads} = -RTLn\left(55.5K_{ads}\right) \tag{6}$$

where R is the gas constant, T is the experiment absolute temperature, and the-constant value of 55.5 is the concentration of water in a solution in mol·L^{-1}. The following equation can be used to calculate a thermodynamic functions [31]

$$\frac{\Delta G^{\circ}_{ads}}{T} = \frac{\Delta H^{\circ}_{ads}}{T} + K \tag{7}$$

The variation of $\Delta G^{\circ}_{ads}/T$ with 1/T gives a straight line with a slope that equals ΔH°_{ads} (Figures 26-28). The $\Delta G^{\circ}_{ads}/T$ decreases with 1/T in a linear manner. The calculated values are shown in Tables 10-12. The adsorption heat could be approximately regarded as the standard adsorption heat under experimental conditions. The negative sign of ΔH°_{ads} in 1M HCl solution indicates that the adsorption of inhibitormolecule is an exothermic process [32]. Then the standard adsorption entropy ΔS°_{ads} was obtained using the thermodynamic basic equation:

$$\Delta G_{ads} = \Delta H_{ads} - \Delta S_{ads} \tag{8}$$

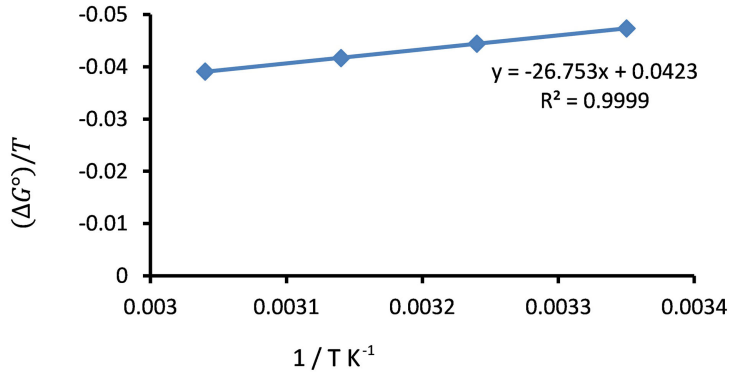

Figure 26. Adsorption isotherm plot for $\Delta G^{\circ}/T$ vs 1/T of GO.

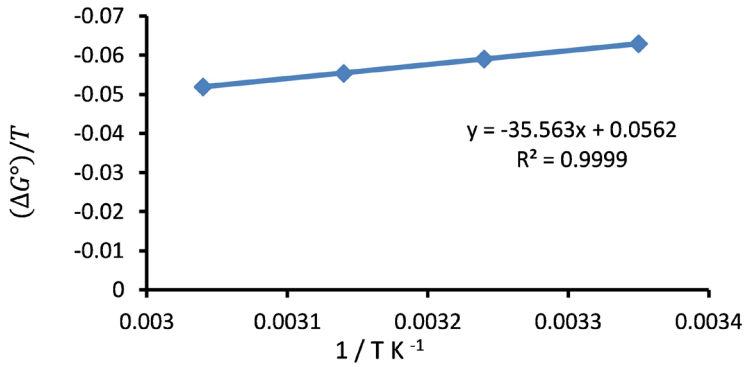

Figure 27. Adsorption isotherm plot for $\Delta G^{\circ}/T$ vs 1/T of GON.

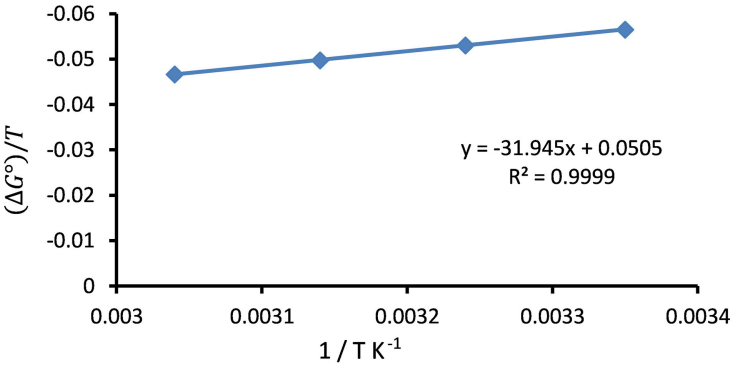

Figure 28. Adsorption isotherm plot for $\Delta G^{\circ}/T$ vs 1/T of GOS.

Table 10. Thermodynamic parameters for the adsorption of GO in 1M HCl on carbon steel surface at different temperatures.

Temperture k	ΔG° (KJ/mol·K)	ΔH° (KJ/mol·K)	ΔS° (J/mol·K)
298	−12.82	−1.30	4.30
308	−13.25	−1.30	4.45
318	−13.68	−1.30	4.59
328	−14.11	−1.30	4.74

Table 11. Thermodynamic parameters for the adsorption of GON in 1N HCl on carbon steel surface at different temperatures.

Temperture k	ΔG° (KJ/mol·K)	ΔH° (KJ/mol·K)	ΔS° (J/mol·K)
298	−17.05	−3.98	5.75
308	−17.62	−3.98	5.91
318	−18.19	−3.98	6.10
328	−18.76	−3.98	6.30

Table 12. Thermodynamic parameters for the adsorption of GOS in 1N HCl on carbon steel surface at different temperatures.

Temperture k	ΔG° (KJ/mol·K)	ΔH° (KJ/mol·K)	ΔS° (J/mol·K)
298	−15.31	−1.30	5.14
308	−15.83	−1.30	5.31
318	−16.34	−1.30	5.48
328	−16.85	−1.30	5.66

4. Conclusion

The grapheme oxide GO, GON, and GOS act as corrosion inhibitors of carbon steel in 1M HCl solutions. The inhibition efficiency increases with increase in inhibitors concentrations and decreases with raising temperature. The adsorption of the investigated compounds follows the Langmuir's adsorption isotherm. The investigated compounds were mixed type inhibitors. The adsorption of the investigated compound is on carbon steel surface in HCl solution. Thermodynamic studied ΔH*, ΔS*, and Ea*, indicated to activity of prepared inhibitors and Free energy of adsorption ΔG°_{ads} indicated to chemical-physical adsorption.

Conflicts of Interest

The authors declare no conflicts of interest regarding the publication of this paper.

References

[1] Dreyer, D.R., Park, S., Bielawski, C.W. and Ruoff, R.S. (2010) The Chemistry of Graphene Oxide. *Chemical Society Reviews*, **39**, 228, https://doi.org/10.1039/B917103G

[2] Chen, M.-L., Meng, Z.-D., Zhu, L., Choi, J.-G., Park, C.-Y., Lee, S.-C., Hong, D.-S., Lee, J.-G., Jang, W.-K. and Oh, W.-C. (2011) Dispersion Stability of Metal (Oxide)-Graphene Nanofluids with Electrical and Thermal Properties. *Science of Advanced Materials*, **3**, 887-892. https://doi.org/10.1166/sam.2011.1213

[3] Zarrok, H., Al-Deyab, S., Zarrouk A., Salghi, Z., Hammouti, B., Oudda, H., Bouachrine, M. and Bentiss, F. (2012) *International Journal of Electrochemical Science*, **7**, 4047.

[4] Khamis, E., Ameer, M.A, Alandis, N.M. and AL-Senani, G. (2000) Effect of Thiosemicarbazones on Corrosion of Steel in Phosphoric Acid Produced by Wet Process. *Corrosion*, **56**, 127-138. https://doi.org/10.5006/1.3280528

[5] Afia, L., Salghi, R., Benali, O., Jodeh, S., Warad, I., Ebenso, E. and Hammouti, B. (2015) *Portugaliae Electrochimica Acta*, **33**, 137.

[6] de Souza, F.S. and Spinelli, A. (2009) Caffeic Acid as a Green Corrosion Inhibitor for Mild Steel. *Corrosion Science*, **51** 642-649. https://doi.org/10.1016/j.corsci.2008.12.013

[7] Hosseini, S.M.A., Salari, M., Jamalizadeh, E., Khezripoor, S. and Seifi, M. (2010) Inhibition of Mild Steel Corrosion in Sulfuric Acid by Some Newly Synthesized Organic Compounds. *Materials Chemistry and Physics*, **119**, 100-105. https://doi.org/10.1016/j.matchemphys.2009.08.029

[8] Popova, A., Sokolova, E., Raicheva, S. and Christov, M. (2003) AC and DC Study of the Temperature Effect on Mild Steel Corrosion in Acid Media in the Presence of Benzimidazole Derivatives. *Corrosion Science*, **45**, 33-58. https://doi.org/10.1016/S0010-938X(02)00072-0

[9] Ramesh, S.V. and Adhikari, A.V. (2009) N'-[4-(Diethylamino)Benzylidine]-3-{[8-(Trifluoromethyl) Quinolin-4-Yl]Thio}Propano Hydrazide) as an Effective Inhibitor of Mild Steel Corrosion in Acid Media. *Materials Chemistry and Physics*, **115**, 618-627. https://doi.org/10.1016/j.matchemphys.2009.01.024

[10] Al Juhaiman, L.A., Mustafa, A.A. and Mekhamer, W.K. (2012) *International Journal of Electrochemical Science*, **7**, 8578.

[11] Alheety, M., Mohammed, M. and Jebour, I. (2016) Synthesis and Haracterization of Novel Nano Dithiocarbamate Complexes Derived From GO-Benzimidazole. *Diyala Journal for Pure Science*, **16**, 108-121.

[12] Shahriary, L. and Athawale, A. (2014) Graphene Oxide Synthesized by Using Modified Hummers Approach. *International Journal of Renewable Energy and Environmental Engineering*, **2**, 58-63.

[13] Paulchamy, B, Arthi, G. and Lignesh, B.D. (2015) A Simple Approach to Stepwise Synthesis of Graphene Oxide Nanomaterial. *Nanomedicine & Nanotechnology*, **6**, 1-4,

[14] Yu, Y., Lin, Y., Lin, C., Chan, C. and Hung, Y. (2014) High-Performance Poly Styrene/Grahene-Based Nano Composites with Excellent Anti-Corrosion Properties. *Polymer Chemistry*, **5**, 535-550, https://doi.org/10.1039/C3PY00825H

[15] Al Juhaiman, L.A. (2016) Polyvinyl Pyrrolidone as a Corrosion Inhibitor for Carbon Steel in HCl. *International Journal of Electrochemical Science*, **11**, 2247-2262.

[16] Chammingkwan, P., Matsushita, K., Taniike, T. and Terano, M. (2016) Enhancement in Mechanical and Electrical Properties of Polypropylene Using Graphene Oxide Grafted with End-Functionalized Polypropylene, *Materials*, **9**, 240. https://doi.org/10.3390/ma9040240

[17] Iram, S. and Hussain, Z. (2015) Covalently Functionalized Graphene Oxide Characterization and Its Electrochemical Performance. *International Journal of Electrochemistry Science*, **10**, 9475-9487.

[18] Monshi, A., Foroughi, M., Monshi, R. and Modified, M.R. (2012) Scherrer Equation to Estimate More Accurately Nano-Crystallite Size Using XRD. *World Journal of Nano Science and Engineering*, **2**, 154-160. https://doi.org/10.4236/wjnse.2012.23020

[19] Theivasanthi, T. and Alagar, M. (2011) Nano Sized Copper Particles by Electrolytic Synthesis and Characterizations. *International Journal of the Physical Sciences*, **6**, 3662-3671.

[20] Meng, F., Ishidab, H. and Liu, X. (2014) Introduction of Benzoxazine onto the Grapheme Oxide Surface by Click Chemistry and the Properties of Graphene Oxide Reinforced Polybenzoxazine Nanohybrids. *RSC Advance*, **4**, 9471-9475. https://doi.org/10.1039/c3ra47345g

[21] Lo, C., Zhu, D. and Jiang, H. (2011) An Infrared-Light Responsive Graphene-Oxide Incorporatedpoly (N-Isopropylacrylamide) Hydrogel Nanocomposite. *Soft Matter*, **7**, 5604-5609. https://doi.org/10.1039/c1sm00011j

[22] Serrar, H., Laroujb, M., Gazc, H.L., Benzekri, Z., Zarguil, A., Essebaai, H., Boukhris, Ouddab, S.H., Salghi, R., Hassikou, A. and Souizi, A. (2018) Experimental and Theoretical Studies of the Corrosion Inhibition of 4-amino-2-(4-chlorophenyl)-8(2, 3-dimethoxyphenyl)-6-oxo-2,6-dihydropyrimido [2,1-b] [1,3] thiazine-3,7 dicarbonitrile on Carbon Steel in a 1.0 M HCl Solution. *Portugaliae Electrochimica Acta*, **36**, 35-52.

[23] Elkhotfi, Y., Forsal, I., Rakib, E.M. and Mernari, B. (2018) The Inhibition Action of Essential Oil of J. Juniperus Phoenicea on the Corrosion of Mild Steel in Acidic Media. *Portugaliae Electrochimica Acta*, **36**, 77-87.

[24] Abdallah, M., Fouad, A., Shama, S. and Afifi, E. (2008) Azodyes as Corrosion Inhibitors for Dissolution of C-Steel in HCl Solution. *African Pure Application Chemistry*, **2**, 83-91.

[25] Al-Sawaad, H.Z.M. (2013) Evaluation of the Ceftriaxone as Corrosion Inhibitor for Carbon Steel Alloy in 0.5 M of Hydrochloric Acid. *International Journal of Electrochemical Science*, **8**, 3105-3120.

[26] Bhat, J. and Alva, V. (2009) Corrosion Inhibition of Aluminium by 2-Chloronicotinic Acid in HCl Medium. *Indian Journal of Chemical Technology*, **16**, 228-233.

[27] Al Juhaiman, L.A. (2016) Polyvinyl Pyrrolidone as a Corrosion Inhibitor for Carbon Steel in HCl. *International Journal of Electrochemical Science*, **11**, 2247-2262.

[28] Dahmani, M., Et-Touhami, A., Al-Deyab, S.S., Hammouti, B. and Bouyanzer, A. (2010) Corrosion Inhibition of C38 Steel in 1M HCl: A Comparative Study of Black Pepper Extract and Its Isolated Piperine. *International Journal of Electrochemical Science*, **5**, 1060-1069.

[29] Abdullah, A. (2008) Adsorption Isotherm of Some Triazoles as Corrosion Inhibitors of Mild Steel in Acids. AL-Fatih, 32.

[30] Abdallah EL, M., Helal, E. and Fouda, A. (2006) *Corrosion Science*, **84**, 1639.

[31] El-Etre, A.Y. (2007) Inhibition of Acid Corrosion of Carbon Steel Using Aqeous

Extract of Olive Leaves. *Journal of Colloid and Interface Science*, **314**, 578-583. https://doi.org/10.1016/j.jcis.2007.05.077

[32] AI-Juaid, S. (2007) Mono Azo Dyes Compounds as Corrosion Inhibitors for Dissolution of Aluminium in Sodium Hydroxide Solutions. *Portugaliae Electrochimica Acta*, **25**, 363-373.